Supporting Information

A Low-temperature Ionic Liquid System to Topochemically Synthesize Si Nanospheres for High-performance Lithium-ion Batteries

*Yanan Xu, Shiyue Zhang, Yu Zhang, Qing Hu, Hao Li, Wenkai Wang, and Hongbin Du**

State Key Laboratory of Coordination Chemistry, School of Chemistry and Chemical Engineering, Nanjing University, Nanjing, 210023, China. E-mail: hbdu@nju.edu.cn

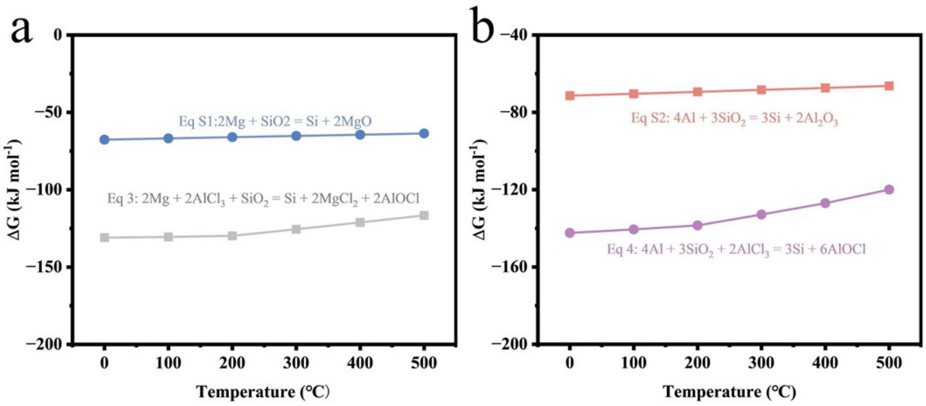

Figure S1. (a-b) The Gibbs free energy curve of the reaction during synthesis.

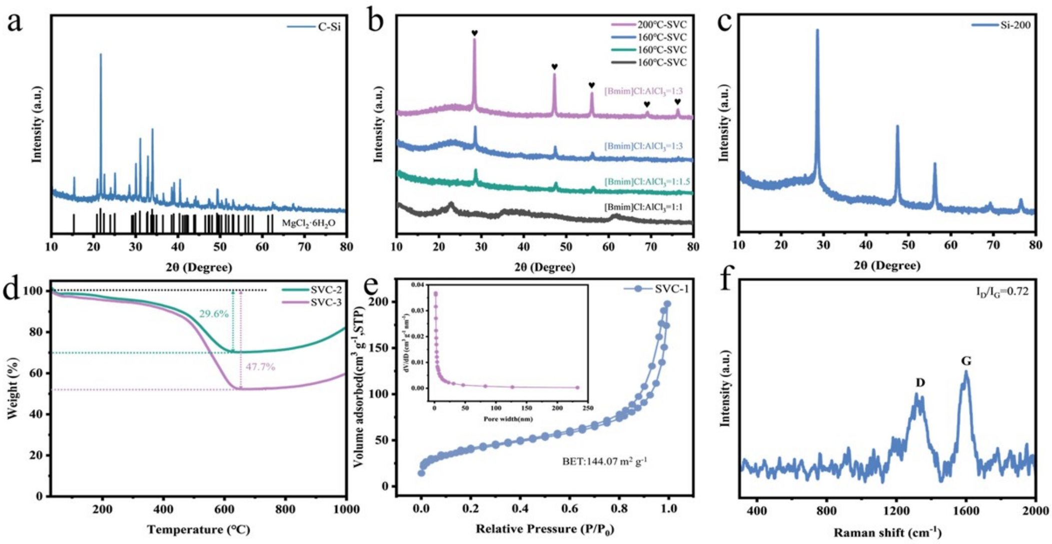

Figure S2. (a) XRD pattern of the crude products after SiO_2@C was reduced. (b) XRD patterns of SVC-1 obtained at 200°C, 160°C, [Bmim]Cl: $AlCl_3$ ratio of 1:1, and 1:1.5, respectively. (c) XRD pattern of Si obtained using $AlCl_3$ as solvent (200 ℃). (d) TGA curves of SVC-2 and SVC-3 (e) N_2 adsorption/desorption isotherms of SVC-1 with inset displaying pore distribution. (f) Raman spectrum of SiO_2@C.

We carried out experiments using $AlCl_3$ as a solvent (without ionic liquid). According to the experimental results, although Si material is also prepared, the reaction temperature must exceed the melting point (194 ℃) to form a solution system. Compared with pure $AlCl_3$ as the reaction medium, the [Bmim]Cl-$AlCl_3$ reaction system is liquid at room temperature, which can disperse the precursor better and has a wider reaction temperature range.

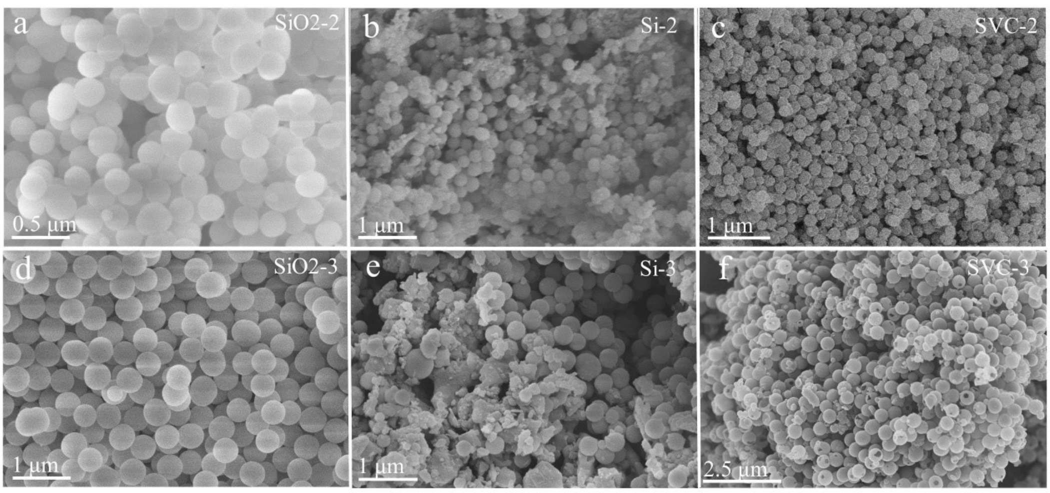

Figure S3. (a-c) SEM images of SiO_2-2, Si-2, and SVC-2. (d-f) SEM images of SiO_2-3, Si-3, SVC-3.

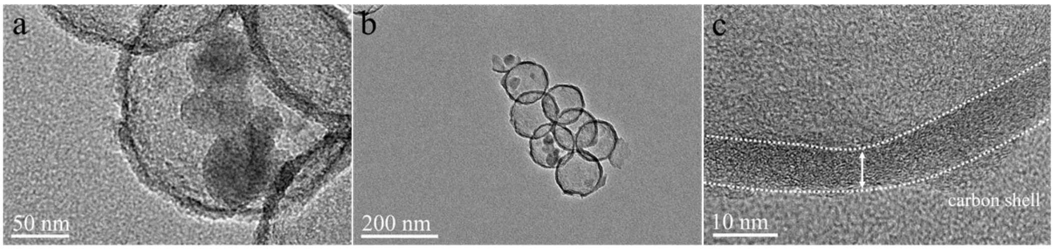

Figure S4. (a-b) TEM image of SVC-1. (c) HRTEM image of SVC-1.

As shown in Figure S4c, the carbon shell of SVC-1 shows an amorphous lattice, which is consistent with the results of XRD result in Figure S2a, indicating that the carbon in SVC-1 exists in an amorphous state.

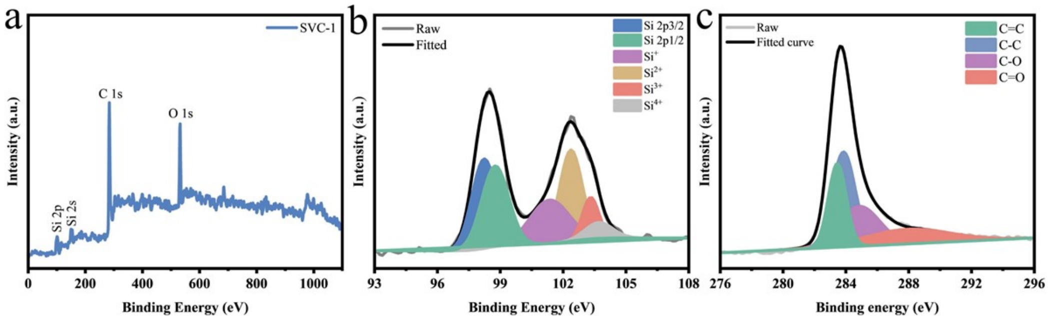

Figure S5. (a) XPS survey spectrum of SVC-1. (b-c) High-resolution XPS fitting results of Si 2p and C 1s.

The high-resolution spectrum of Si reveals six characteristic peaks, confirming the existence of Si $2p_{3/2}$ (98.3 eV), Si $2p_{1/2}$ (98.8 eV), Si^{+} (101.4 eV), Si^{2+} (102.4 eV), Si^{3+} (103.3 eV), and Si^{4+}(103.9 eV).

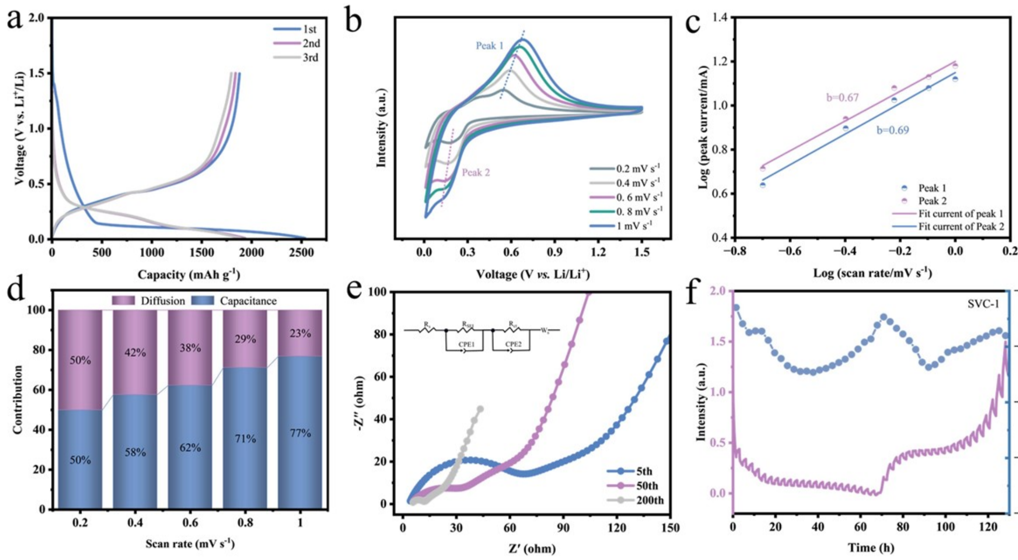

Figure S6. (a) The capacity-voltage curves of SVC-1. (b) CV curves of ns-Si at different scan rates and (c) the corresponding log (|*i*|) versus log (*v*) plots. (d) Capacity contribution of ns-Si for pseudo-capacitance control and diffusion control at different scan rates. (e) Equivalent circuits and EIS curves of ns-Si after the 5th, 50th, and 200th cycles. (f) GITT curve of SVC-1.

Table S1. A summary of the performances of reported Si electrodes

Materials	Preparative Method	ICE	Current density	Cycles	Capacity after cycles (mA h g^{-1})	Capacity retention	Reference
Si/SiOx	Magnesiothermic reduction	68%	0.2 A g^{-1}	100	1400	98%	1
Si@SiO_2	Magnesiothermic reduction	63.8%	0.36A g^{-1}	100	1470	82.5%	2
Si-200	MgH_2 reduction	85.7%	2 A g^{-1}	500	854	<30.0%	3
p-SiNPs@HC-1	Magnesiothermic reduction	55%	0.2 A g^{-1}	100	1436	83.0%	4
Si/C/Si/C	Aluminothermic reduction	83.1%	1 A g^{-1}	200	1673	86.9%	5
Nano-Si	Aluminothermic reduction	81.7%	0.5 A g^{-1}	500	2663	<80%	6
3-D Si	Magnesiothermic reduction	74%	0.4 A g^{-1}	400	1287	52%	7
Si/C	Mg/Al reduction	65%	0.2 A g^{-1}	100	600	71.3%	8
Si/SiC/C	Magnesiothermic reduction	79.1%	0.1 A g^{-1}	200	13290	87.8%	9
Hierarchical Si	Magnesiothermic reduction	xxx	1 A g^{-1}	100	500	75%	10
HPS-Si	Magnesiothermic reduction	62.7%	0.2 A g^{-1}	100	1272.8	xxx	11
Si/C	Magnesiothermic reduction	73.2%	0.2 A g^{-1}	100	1449.2	98%	12
Si@C	Magnesiothermic reduction	<54%	0.1 A g^{-1}	100	1546	<99%	13
SiOC-H.	Magnesiothermic reduction	70%	2 A g^{-1}	400	<600	<50%	14
Nano-Si	Magnesiothermic reduction	82.9%	0.5 A g^{-1}	100	2021.2	92.4%	***This work***
SVC-1	Magnesiothermic reduction	74.1%	0.5 A g^{-1}	100	1454.7	100%	***This work***
			2 A g^{-1}	600	913.7	73.9%	***This work***

Table S2. EIS fitting parameters of commercial ns-Si and SVC-1 before cycling.

Sample	$R_s(\Omega)$	R_{ct}（Ω）
ns-Si	3.1	131.6
SVC-1	2.6	121.1

Table S3. EIS fitting parameters of SVC-1 at 5th, 50th, and 200th.

Sample	$R_s(\Omega)$	R_{SEI}	R_{ct}（Ω）
5th	3.4	59.9	52.9
50th	4.2	33.3	33.6
200th	4.9	7.2	12.9

References

1 K. Zeng, T. Li, X. Y. Qin, G. M. Liang, L. H. Zhang, Q. Liu, B. H. Li and F. Y. Kang, *Nano Res*, 2020, **13**, 2987-2993.

2 J. W. Liang, X. N. Li, Z. G. Hou, W. Q. Zhang, Y. C. Zhu and Y. T. Qian, *ACS Nano*, 2016, **10**, 2295-2304.

3 J. G. Yu, K. Wang, W. L. Song, H. Huang, C. Liang, Y. Xia, J. Zhang, Y. P. Gan, F. Wang and W. K. Zhang, *Chem. Eng. J.* 2021, **406**, 126805.

4 S. C. Guo, X. Hu, Y. Hou and Z. H. Wen, *ACS Appl. Mater. Interfaces*, 2017, **9**, 2084−42092.

5 H. M. Wu, P. B. Gao, J. l. Mu, Z. C. Miao, P. F. Zhou, T. Zhou and J. Zhou, *Chinese Chem. Lett*, 2022, **33**, 3236–3240.

6 N. Lin, Y. Han, J. Zhou, K. Zhang, T. Xu, Y. Zhu and Y. Qian, *Energy Environ Sci*, 2015, **8**, 3187-3191.

7 A. Ansari Hamedani, C. W. Ow-Yang and S. Hayat Soytas, *ChemElectroChem*, 2021, **8**, 3181-3191.

8 M. K. Majeed, A. Saleem, C. S. Wang, C. H. Song and J. Yang, *Chem-eur J*, 2020, **26**, 10544-10549.

9 X. H. Huang, R. Q. Guo, Y. Lin, Y. Q. Cao and J. B. Wu, *J Energy Storage*, 2024, **87**, 111374.
10 J. K. Yoo, J. Kim, M. J. Choi, Y. U. Park, J. Hong, K. M. Baek, K. Kang and Y. S. Jung, *Adv Energy Mater*, 2014, **4**, 1400622.
11 F. Di, Z. X. Wang, C. Ge, L. X. Li, X. Geng, C. G. Sun, H. M. Yang, W. M. Zhou, D. Y. Ju, B. G. An and F. Li, *Journal of Materials Science & Technology*, 2023, **157**, 1-10.
12 X. J. Lin, A. Li, D. Li, H. H. Song and X. H. Chen, *ACS Applied Materials & Interfaces*, 2020, **12**, 15202-15210.
13 Q. Liu, Y. X. Ji, X. M. Yin, J. W. Li, Y. J. Liu, X. Hu and Z. H. Wen, *Energy Storage Mater*, 2022, **46**, 384-393.
14 S. J. Yeom, T.-U. Wi, S.-J. Jung, M. S. Kim, S.-C. Jeon and H.-W. Lee, *Chem Commun*, 2023, **59**, 11963-11966.